Measurement of the neutron total cross section of carbon at the Back-n white neutron beam of CSNS

Xing-Yan Liu[1] · Yi-Wei Yang[1] · Rong Liu[1] · Jie Wen[1] · Zhong-Wei Wen[1] ·
Zi-Jie Han[1] · Zhi-Zhou Ren[1] · Qi An[2,3] · Huai-Yong Bai[4] · Jie Bao[5] ·
Ping Cao[2,3] · Qi-Ping Chen[1] · Yong-Hao Chen[6,7] · Pin-Jing Cheng[8] ·
Zeng-Qi Cui[4] · Rui-Rui Fan[2,6,7] · Chang-Qing Feng[2,3] · Min-Hao Gu[2,6] ·
Feng-Qin Guo[6,7] · Chang-Cai Han[9] · Guo-Zhu He[5] · Yong-Cheng He[6,7] ·
Yue-Feng He[8] · Han-Xiong Huang[5] · Wei-Ling Huang[6,7] · Xi-Ru Huang[2,3] ·
Xiao-Lu Ji[2,6] · Xu-Yang Ji[2,10] · Hao-Yu Jiang[4] · Wei Jiang[6,7] · Han-Tao Jing[6,7] ·
Ling Kang[6,7] · Ming-Tao Kang[6,7] · Bo Li[6,7] · Lun Li[6,7] · Qiang Li[6,7] ·
Xiao Li[6,7] · Yang Li[2,6] · Yang Li[6,7] · Shu-Bin Liu[2,3] · Guang-Yuan Luan[4] ·
Ying-Lin Ma[6,7] · Chang-Jun Ning[6,7] · Bin-Bin Qi[3] · Jie Ren[5] · Xi-Chao Ruan[5] ·
Zhao-Hui Song[9] · Hong Sun[6,7] · Xiao-Yang Sun[6,7] · Zhi-Jia Sun[2,6,7] ·
Zhi-Xin Tan[6,7] · Hong-Qing Tang[5] · Jing-Yu Tang[6,7] · Peng-Cheng Wang[6,7] ·
Qi Wang[5] · Tao-Feng Wang[12] · Yan-Feng Wang[6,7] · Zhao-Hui Wang[5] ·
Zheng Wang[6,7] · Qing-Biao Wu[6,7] · Xiao-Guang Wu[5] · Xuan Wu[6,7] ·
Li-Kun Xie[2,10] · Han Yi[6,7] · Li Yu[2,3] · Tao Yu[2,3] · Yong-Ji Yu[6,7] · Guo-Hui Zhang[4] ·
Jing Zhang[6,7] · Lin-Hao Zhang[6,7] · Li-Ying Zhang[2,6,7] · Qing-Min Zhang[11] ·
Qi-Wei Zhang[5] · Xian-Peng Zhang[9] · Yu-Liang Zhang[6,7] · Zhi-Yong Zhang[2,3] ·
Ying-Tan Zhao[11] · Liang Zhou[6,7] · Zu-Ying Zhou[5] · Dan-Yang Zhu[3] ·
Ke-Jun Zhu[2,6] · Peng Zhu[6,7]

Abstract To verify the performance of the neutron total cross-sectional spectrometer, the neutron total cross section of carbon is initially measured in the energy range of 1 eV to 20 MeV using the time-of-flight method. The measurement is performed at the Back-n white neutron source with a 76-m time-of-flight path using the China Spallation Neutron Source. A multilayer fast fission chamber with ^{235}U and ^{238}U is employed as the neutron detector. The diameter and thickness of the natural graphite sample are 70 mm and 40 mm, respectively. Signal waveforms are

✉ Rong Liu
liurongzy@163.com

[1] Institute of Nuclear Physics and Chemistry, China Academy of Engineering Physics, Mianyang 621900, China

[2] State Key Laboratory of Particle Detection and Electronics, Chinese Academy of Sciences (CAS), Beijing 100049, China

[3] Department of Modern Physics, University of Science and Technology of China, Hefei 230026, China

[4] State Key Laboratory of Nuclear Physics and Technology, School of Physics, Peking University, Beijing 100871, China

[5] Key Laboratory of Nuclear Data, China Institute of Atomic Energy, Beijing 102413, China

[6] Institute of High Energy Physics, Chinese Academy of Sciences (CAS), Beijing 100049, China

[7] Spallation Neutron Source Science Center, Dongguan 523803, China

[8] University of South China, Hengyang 421001, China

[9] Northwest Institute of Nuclear Technology, Xi'an 710024, China

[10] Department of Engineering and Applied Physics, University of Science and Technology of China, Hefei 230026, China

[11] Xi'an Jiaotong University, Xi'an 710049, China

[12] Beihang University, Beijing 100083, China

collected using a data acquisition system. Off-line data processing was used to obtain the neutron time-of-flight spectra and transmissions. The uncertainty of the counting statistics is generally approximately 3% for each bin in the energy range of 1–20 MeV. It is determined that the results for the neutron total cross section of carbon obtained using ^{235}U cells are in good agreement with the results obtained using ^{238}U cells within limits of statistical uncertainty. Moreover, the measured total cross sections show good agreement with the broadening evaluated data.

Keywords CSNS · Back-n white neutron source · NTOX · Neutron total cross section · Carbon · Multilayer fast fission chamber

1 Introduction

The neutron total cross section is a basic quantity for describing the interactions between neutrons with nuclei and is defined as the sum of the probabilities of the interactions of neutrons with nuclei. It provides basic information about the internal structure of the nuclei and its constituents and plays an important role in the development and application of nuclear science and technology. High-accuracy neutron total cross-sectional measurements are necessary to design nuclear devices. Since the 1970s, a large amount of neutron total cross-sectional data in the energy range of 5 eV to 20 MeV has been obtained via a transmission method at the Oak Ridge Electron Linear Accelerator (ORELA) [1]. With the development of nuclear technology, the measurement method has improved and the detectable energy range of neutrons has expanded. Since the 1990s, numerous neutron total cross-sectional measurements have been performed with white neutron sources. The total cross section of carbon and its resonances are very well known [2]. Therefore, it can be used as a reliable standard to evaluate the efficacy of a measurement method. Finlay et al. [3] measured $\sigma_T(E)$ in the neutron energy region, up to 600 MeV for carbon at the Los Alamos National Laboratory (LANL) "white" neutron facility using BC404, and the statistical uncertainty was better than 1% for each of several hundred energy bins. The investigators used the resonances of carbon to fit the neutron flight path. Abfalterer et al. [4] successfully obtained the total cross-sectional measurement of natural carbon in the neutron energy region from 0.75 to 11.3 MeV at the LANL using a NE213 liquid scintillator, and the statistical uncertainty was better than 2% over the entire energy range. Abfalterer et al. [5] measured $\sigma_T(E)$ in the neutron energy range of 5–600 MeV for carbon at the LANL using BC404. Danon et al. [2] investigated the use of the filtered beam method to measure $\sigma_T(E)$ in the

neutron energy range of 24–940 keV for carbon at Rensselaer Polytechnic Institute (RPI). Rapp et al. [6] evaluated the feasibility of determining the neutron total cross section of a detection system based on measurements of $\sigma_T(E)$ of natural carbon in the energy range of 0.4–20 MeV.

The China Spallation Neutron Source (CSNS) is a large scientific facility that was completed in May 2018 [7–9]. The present experiment was conducted at the Back-n white neutron beam line of the CSNS (CSNS-WNS) which can generate a high-flux neutron beam that covers a wide energy range from thermal to hundreds of mega-electron-volts [10].

In the present work, a technique for measuring neutron total cross section is developed using the neutron total cross-sectional spectrometer (NTOX) based on a multilayer fast fission chamber with ^{235}U and ^{238}U at the CSNS-WNS. The measurement of the neutron total cross sections of carbon within the energy range of 1 eV to 20 MeV was performed using the time-of-flight method. The presented results are compared with the evaluated data from ENDF/B-VIII.0 [11] to evaluate the performance of NTOX.

2 Experimental method

Neutron total cross sections are determined by measurement of the transmission, which is the ratio of the neutron counts for an open beam and the sample-in. This parameter can be calculated as follows:

$$\sigma(E_i) = -\frac{1}{nl}\ln T(E_i), \tag{1}$$

where nl is the number of atoms per unit area of the sample, $T(E_i)$ is the transmission of the neutrons for the i-th group energy E_i. This parameter is not related to the efficiency of a given detector and is described as follows:

$$T(E_i) = \frac{I_I(E_i)/P_I}{I_O(E_i)/P_O}. \tag{2}$$

$I_I(E_i)$ and $I_O(E_i)$ are the neutron counts for the sample-in and the open beam and P_I and P_O are proton counts for the sample-in and the open beam, respectively. The transmission is measured using a multilayer fast fission chamber with ^{235}U and ^{238}U with standard fission cross sections [12, 13]. Given that the chamber has no gamma-background effect, it is ideal for use as a neutron detector for total cross-sectional measurements at the CSNS-WNS.

To reduce the influence of neutron scattering and to improve the accuracy of the measurement, the diameter of the cylindrical sample should be larger than the beam spot diameter and the shadow of the sample should completely cover the front of the detector. The neutron energy is measured via a time-of-flight method.

The neutrons were produced by spallation of a 1.6 GeV proton beam with a beam power of 20 kW, a pulse frequency of 25 Hz and a pulse width of 50 ns incident on a tungsten target at the CSNS [14]. The neutron source has two modes: a single mode and a double mode. The measurement was performed in the double mode with an interval between the two bunches of approximately 410 ns, whereby the full width at half maximum (FWHM) of a bunch is 50 ns. The white neutron spectrum is shown in Fig. 1.

3 Ntox

NTOX was established as a spectroscopic approach for high-precision measurement of the neutron total cross section of some elements. It consists of a multilayer fast fission chamber, front-end electronics, data acquisition (DAQ) and a sample changer. Based on the CSNS-WNS and multilayer fast fission chamber, the neutron total cross sections can be obtained in a wide energy region in a single measurement and more neutrons can be measured in a short time.

3.1 Experimental arrangement

The arrangement for the total cross-sectional experiment should exhibit "good geometry," including the target, collimators, sample changer and neutron detector, as shown in Fig. 2. Two experimental stations, i.e., Endstation#1 and #2, are constructed in the neutron beam line [10]. A sample changer that can hold several samples is located at Endstation#1. The neutron detector is at Endstation#2, which is a distance of approximately 76 m from the spallation target. The distance between the sample and the detector is approximately 20 m. The scattered neutrons
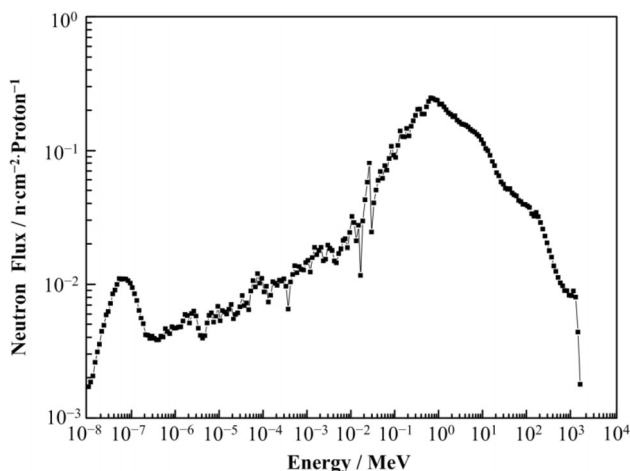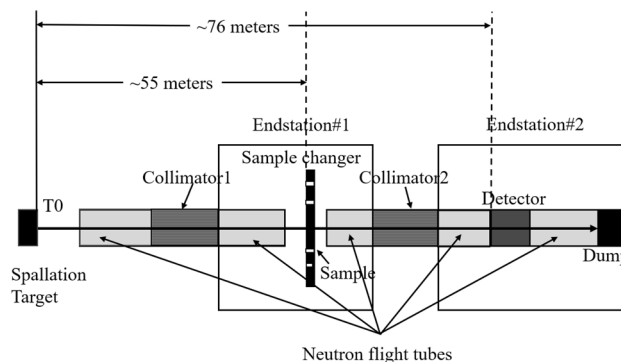

Fig. 2 Geometry for the present experiment [10]

can be reduced for this distance and good collimation between the sample and the detector.

There are two collimators in the neutron beam line, and their diameters can be selected. The diameter of the detector is 50 mm, and the diameter of collimator 2 is set to be 30 mm, whereas the diameter of collimator 1 is 60 mm.

3.2 Detection system

A multilayer fast ionization chamber is located in the neutron beam line at Endstation#2, as shown in Fig. 3 [16]. Three ^{235}U and three ^{238}U cells are located in the detector. By counting and analyzing the fission events of ^{235}U(n, f) and ^{238}U(n, f) reactions, the neutron counts can be determined.

The fission signal was collected by the MSI-8 preamplification, and the Back-n public DAQ system was developed by the University of Science and Technology of China. The DAQ system mainly includes an SCM module (signal conditioning module), an FDM module (field digitizing module), a TCM module (trigger and clock module) and a data center for storing waveform data [17]. The start signal of the FDM module is provided by the TCM, and the trigger signal of the TCM is provided by the external T0 signal. This signal originates from the accelerator proton target signal.

The block diagram of the entire detection system is shown in Fig. 4. The proton monitor at the CSNS is used to measure the proton count, which is then used to normalize the neutron count. The acquired neutron signals are then saved in the DAQ data center for off-line processing after the experiment is completed. The UTC of each proton pulse corresponds to that of every event number in the DAQ data center.

3.3 Sample

To increase the accuracy of the measurements, the number of scattered neutrons must be minimized. The main
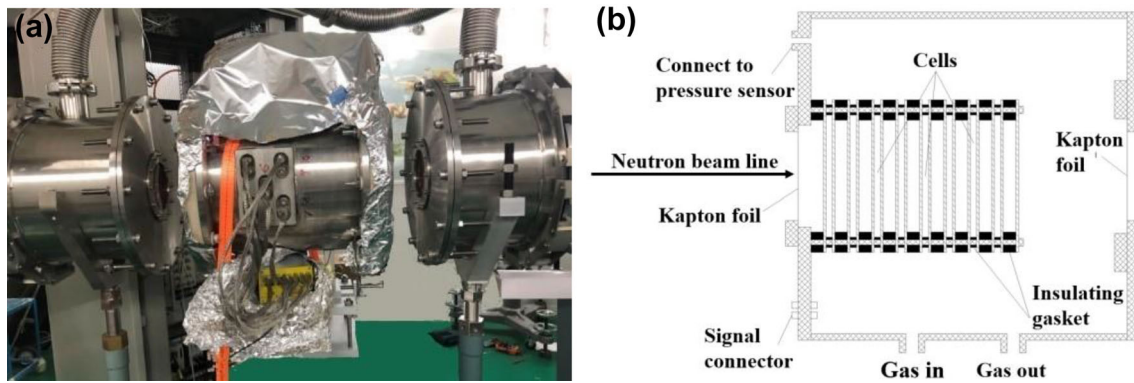

Fig. 1 Energy spectrum of the CSNS-WNS [15]

Fig. 3 A photograph of the FIC (**a**) and the schematic view (**b**), **b** from Ref. [16]. In **b**, from left to right, the cells are Fe, U238-1, U235-1, U235-2, U238-2, U, U235-3 and U238-3, respectively
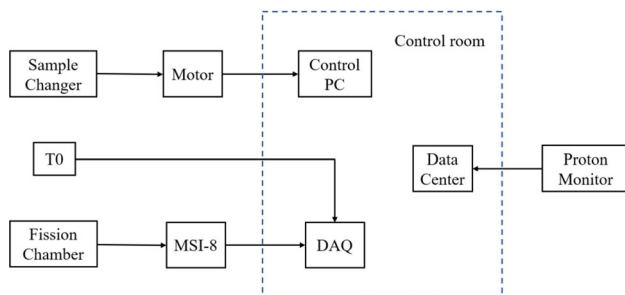

Fig. 4 Block diagram of the detection system

contribution of the scattered neutrons depends on the size of the sample and its position in the NTOX. Considering the scattering process, the sample should be smaller and thinner. A thick sample should be selected if the statistics of the neutron counts are emphasized. Taking both factors into consideration, a T of 0.5–0.7 is preferred in the actual measurement [18].

A simulation based on the Monte Carlo N-Particle (MCNP) code was performed to determine the thickness of the sample. The sample used in this work was a cylindrical natural graphite. The results indicate that the neutron energy range corresponding to a transmission of 0.5–0.7 is 2–20 MeV when the graphite sample is 40 mm thick and the total cross section of the resonance region in carbon is more desirable. The physical parameters of the sample used in the experiment are given in Table 1. The calculated density of the sample was 1.86 g/cm^3, which is lower than the normal graphite density (2.25 g/cm^3). Preliminary judgment is that this 17% difference is caused by the

Table 1 Physical parameters of the sample used in the experiment

Sample	Diameter (mm)	Thickness (mm)	Mass (g)
Graphite	70.07 ± 0.02	40.03 ± 0.02	287.79 ± 0.01

production process. Therefore, the atomic density (0.3741 atoms/barn) should be an apparent value.

A sample changing system was used to change the sample's position in a few seconds, as shown in Fig. 5. The sample holders can mount several samples, and they are positioned at the top of the sample changer. In addition, they can be driven horizontally and vertically. By centering a sample before measurements are performed and recording the data at the center of a neutron beam, samples could be moved to the expected positions using a motor controlled by a computer in the control room. The positioning accuracy is 0.001 mm.

4 Results

The total data acquisition time for the graphite sample was 32.4 h, and the total time for the open beam was 14.6 h. The experimental data can be analyzed using a C++ program and Root [19]. The raw data could be decoded to Root files that contain amplitude and time information of the signals, and then this information could be extracted using the C++ program.
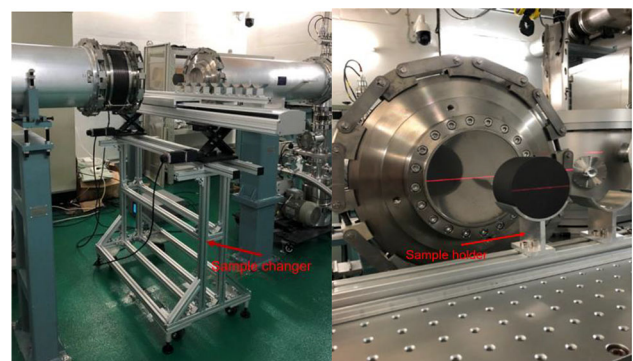

Fig. 5 Sample changer

4.1 Amplitude spectra

The amplitude distributions of the ^{235}U and ^{238}U fission cells in addition to the measured backing and alpha signals are shown in Fig. 6. The signal amplitude is mainly due to α-particle decay and electronic noise, and it must be subtracted from the neutron spectrum. The threshold could be determined by analyzing the amplitude spectrum. It is the center of the amplitude spectrum valley.

4.2 Energy calibration

The neutron energy E_n is given as follows:

$$E_n = m_n c^2 \left(\frac{1}{\sqrt{1 - \beta_n^2}} - 1 \right), \tag{3}$$

where m_n is the mass of a neutron and c is the speed of light,

$$\beta_n = \frac{v_n}{c} = \frac{L}{c \mathrm{Tof}}$$

where v_n is the neutron speed, L is the length of the flight path and Tof is the neutron time of flight, which is given as follows:

$$\mathrm{Tof} = T_{ff} + \mathrm{Tof}_{gamma} - T_{gamma}, \tag{4}$$

where T_{ff} is the start time of the fission signal recorded via the DAQ system and T_{gamma} is the start time of the gamma-flash recorded by this system. It is obtained by measuring gamma-flash at the 90-mm neutron beam window at 2 atm. The details of the measurement method will be presented in another report. Tof_{gamma} is the gamma-ray time of flight for the flight path, $\mathrm{Tof}_{gamma} = L/c$. By substituting for Tof and solving for $T_{ff} - T_{gamma}$, we have:

$$T_{ff} - T_{gamma} = \frac{L}{c} \left[\frac{1}{\sqrt{1 - \frac{1}{\left(\frac{E_n}{m_n c^2} + 1 \right)^2}}} - 1 \right]. \tag{5}$$

Using a known approximate flight path of 76 m to obtain a neutron time-of-flight spectrum and then comparing to the one calculated using ENDF/B-VIII.0 [12], the 8.77 eV resonance is determined. By performing a Gaussian fit of the 8.77 eV resonance of ^{235}U in this work, $T_{ff} - T_{gamma}$ is determined to be 1,853,660 $\pm$ 20 ns. Substituting into Eq. (5), a neutron flight path of 75.939 m of the first ^{235}U fission cell can be obtained.

Using the signal for the first ^{235}U fission cell for sample-in based on the same method, a flight path of 75.938 m is obtained. This value has a difference of 0.013‰ compared to 75.939 m. Similarly, the neutron flight path of the other two ^{235}U fission cells can be obtained. By using the ^{235}U and ^{238}U fission cell geometric distance, the neutron flight path of the three ^{238}U fission cells can also be obtained, as shown in Table 2.

The uncertainty of the flight path is less than 0.04‰. The difference between the distance between the two fission cells obtained by calculation and the actual geometric distance of the two fission cells is within the uncertainty of the flight path.

If the time of flight is known based on Eq. (4) and the flight path, the neutron energy spectrum can be obtained. Figure 7 shows the amplitude energy two-dimensional distribution of the first ^{235}U cell when open beam (a) and sample-in (b). When the neutron energy is below 300 keV, there is an amplitude boundary of approximately 250 ch between the fission and α-particle signal in the distribution. When neutron energy is in the range of 300 keV–10 MeV,
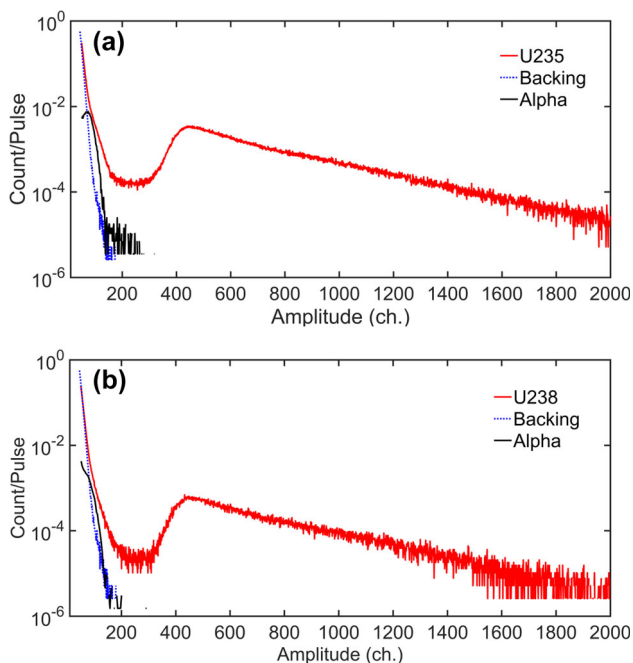

Fig. 6 Amplitude distributions of ^{235}U (a) and ^{238}U (b) cells under open beam

Table 2 The neutron flight path with all of the fission cells

Cells	T_{gamma} (ns)	L (m)	Tof_{gamma} (ns)
U238-1	− 574.8	75.921	253.2
U235-1	− 574.8	75.939	253.3
U235-2	− 573.9	75.957	253.4
U238-2	− 572.7	75.975	253.4
U235-3	− 575.1	76.011	253.5
U238-3	− 574.7	76.029	253.6
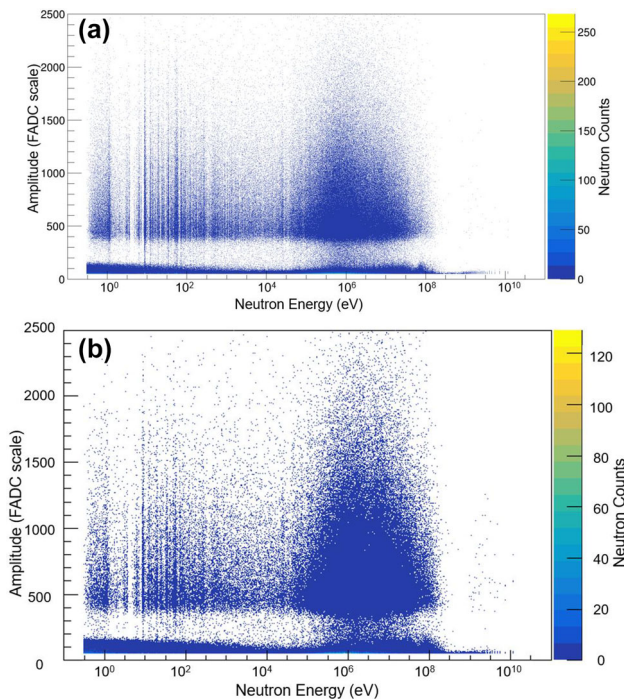
Fig. 7 Amplitude–energy 2D distribution map of the first ^{235}U cell for open beam (**a**) and sample-in (**b**)

Fig. 8 The normalized neutron energy spectrum with the first ^{235}U fission cell (**a**) and the first ^{238}U fission cell (**b**)

Fig. 9 Measured transmission of carbon with the first ^{235}U fission cell (**a**) and the first ^{238}U fission cell (**b**)

the boundary is relatively blurred. This is because of the large number of fission events and high-energy α-particle events generated by (n, α) reaction.

The neutron energy spectra for which the neutron count is normalized by the proton count can be obtained using Eq. (3), as shown in Fig. 8. To increase the statistical count of the low-energy region, the bin is larger than that the case when the flight distance (1000 ns/bin) is determined and is divided by log (eV) with 100 bins for each order.

4.3 Total cross section

Using Eq. (2), the transmission with the first ^{235}U and ^{238}U fission cell can be obtained based on the normalized energy spectrum, as shown in Fig. 9.

The neutron total cross sections with three ^{235}U and three ^{238}U fission cells can be obtained using Eq. (1), as shown in Fig. 10. The large statistical fluctuation within the energy range of 3–30 eV in Fig. 10a is derived from insufficient neutron counts ($\sim$ 20 counts/bin) with one fission cell.

To increase the statistical count, the count with three identical fission cells can be added. The transmission with ^{235}U and ^{238}U fission cells can be calculated after the neutron count is added as follows:
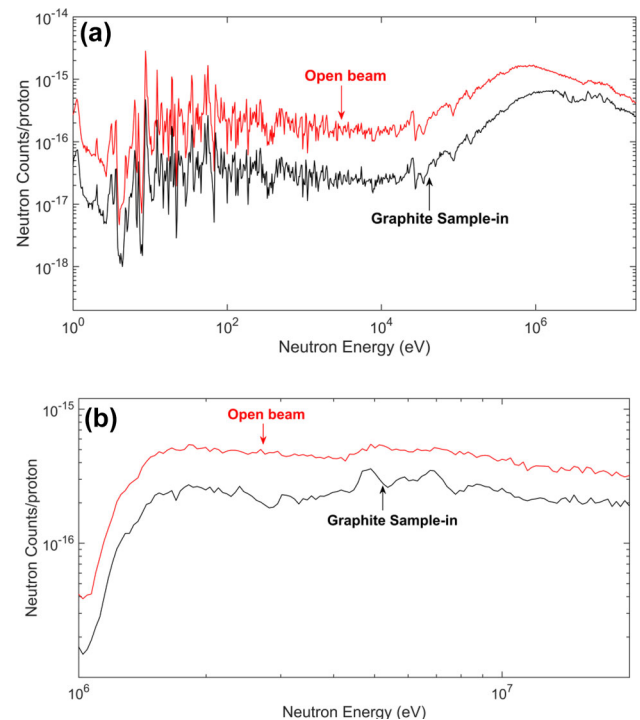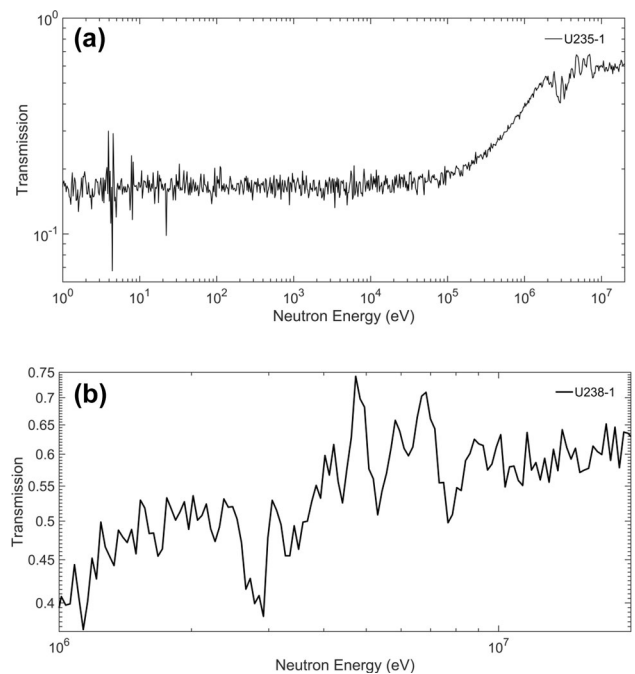
Fig. 10 The neutron total cross section with ^{235}U (**a**) and ^{238}U (**b**) fission cells

Table 4 The detection efficiency of fission cells

Fission cell	Fission count efficiency (%)
U235-1	94.91
U235-2	95.03
U235-3	93.93
U238-1	94.43
U238-2	95.42
U238-3	94.81

$$T(E_i)_5$$
$$= \frac{[I_I(E_i)_{51}/(\eta_{51}m_{51}) + I_I(E_i)_{52}/(\eta_{52}m_{52}) + I_I(E_i)_{53}/(\eta_{53}m_{53})]/P_I}{[I_O(E_i)_{51}/(\eta_{51}m_{51}) + I_O(E_i)_{52}/(\eta_{52}m_{52}) + I_O(E_i)_{53}/(\eta_{53}m_{53})]/P_O}$$
(6)

$$T(E_i)_8$$
$$= \frac{[I_I(E_i)_{81}/(\eta_{81}m_{81}) + I_I(E_i)_{82}/(\eta_{82}m_{82}) + I_I(E_i)_{83}/(\eta_{83}m_{83})]/P_I}{[I_O(E_i)_{81}/(\eta_{81}m_{81}) + I_O(E_i)_{82}/(\eta_{82}m_{82}) + I_O(E_i)_{83}/(\eta_{83}m_{83})]/P_O},$$
(7)

where $I_I(E_i)_{51}$, $I_I(E_i)_{52}$ and $I_I(E_i)_{53}$ are the neutron counts for the sample-in, $I_O(E_i)_{51}$, $I_O(E_i)_{52}$ and $I_O(E_i)_{53}$ are the neutron counts for the open beam with U235-1, U235-2 and U235-3, respectively, η_{51}, η_{52} and η_{53} are the fission count efficiency, and m_{51}, m_{52} and m_{53} are the effective mass for detecting neutrons of ^{235}U. $T(E_i)_8$ is the transmission with ^{238}U fission cells after superimposing the neutron count.

The neutron count ratio with all the fission cells and the uranium mass ratio for every fission cell are shown in Table 3. The uncertainty of the uranium mass is

approximately 1%. The difference between the neutron count ratio with a fission cell and the mass ratio of uranium is less than 3%. Therefore, the nonuniformity of the uranium distributed on the backing is negligible and the uranium mass can be used in Eqs. 6 and 7 instead of the effective mass. The fission count efficiency and the uranium mass should be only considered when neutron counts are added.

The fission count efficiency of fission cells can be seen in Table 4. The details of the fission count efficiency calculations will be presented in a separate report.

After the addition, the neutron total cross section with ^{235}U and ^{238}U fission cells is as shown in Fig. 11. The statistical uncertainty is less than that with one cell.

As shown in Table 5, the neutron statistical uncertainty for each bin with ^{235}U fission cells is different in different energy regions. Compared to one cell of the ^{235}U fission cells, the neutron statistical uncertainty is reduced by approximately 45% with three superimposed ^{235}U fission cells.

The neutron statistical uncertainty for each bin with ^{238}U fission cells is shown in Table 6. Compared to one piece of ^{238}U fission cell, the neutron statistical uncertainty is reduced by approximately 42% with three superimposed ^{238}U fission cells.

5 Data analysis

5.1 ^{235}U(n, f) resonance peak

The fission count-neutron energy spectrum is compared with the fission cross section from ENDF/B-VIII.0 in Fig. 11. There is a good agreement for all the fission
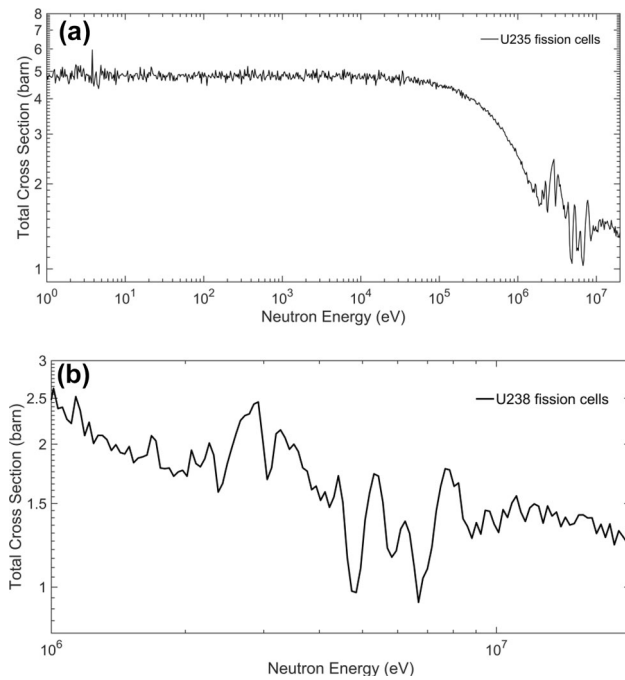
Table 3 The neutron count ratio and the uranium mass ratio for fission cells

Fission cell	Mass ratio	Neutron count ratio		Difference between the two ratios	
		Open beam	Sample-in	Open beam (%)	Sample-in (%)
U235-2 and U235-1	1.10	1.10	1.10	0.55	0.58
U235-3 and U235-1	1.09	1.06	1.06	2.96	3.00
U238-2 and U238-1	1.00	0.99	0.99	0.42	0.43
U238-3 and U238-1	0.95	0.93	0.93	1.22	1.29

Fig. 11 The neutron total cross section with ^{235}U and ^{238}U fission cells after adding the neutron counts

Table 5 Neutron statistical uncertainty with ^{235}U fission cells

Energy	Statistical uncertainty per bin	
1 eV to 1.5 keV	One fission cell	2.56–50.10%
	Three fission cells	1.44–29.14%
1.5 keV to 1 MeV	One fission cell	2.68–16.07%
	Three fission cells	1.52–8.72%
1–2 MeV	One fission cell	2.68–2.94%
	Three fission cells	1.52–1.66%
2–20 MeV	One fission cell	2.94–3.78%
	Three fission cells	1.66–2.11%

Table 6 Neutron statistical uncertainty with ^{238}U fission cells

Energy	Statistical uncertainty per bin	
1–2 MeV	One fission cell	4.56–17.63%
	Three fission cells	2.66–9.87%
2–20 MeV	One fission cell	4.22–5.58%
	Three fission cells	2.43–3.23%

resonances in the energy range of 5–20 eV, and only a few differences in some detail structures are observed. In addition to the 8.77 eV resonance peak, there is a good
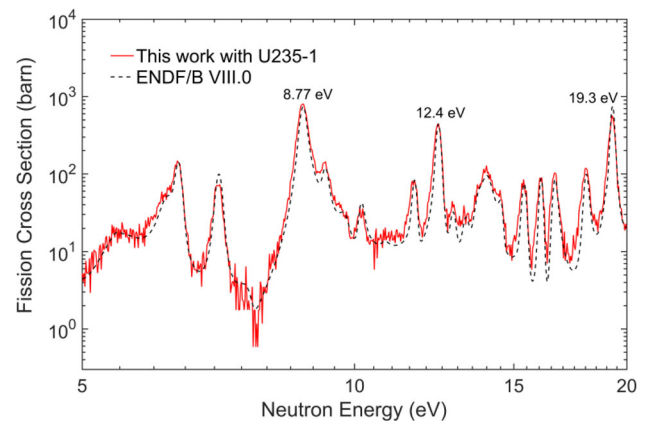

Fig. 12 The neutron energy spectrum measured with the first ^{235}U cell (open beam) compared to the evaluated data
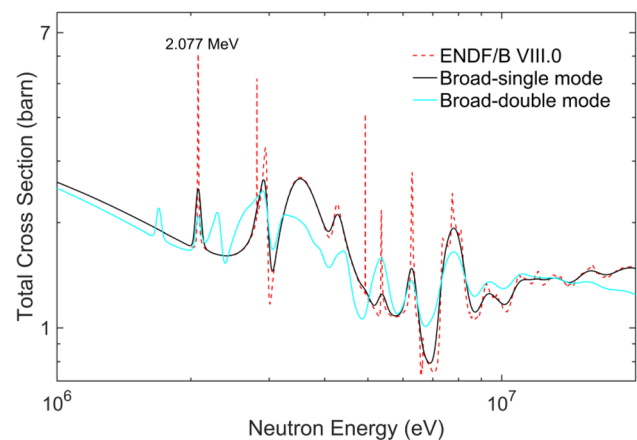

Fig. 13 Gaussian broadening for single-mode (red line) and double-mode (blue line) neutron beams on the cross section of the evaluated data. (Color figure online)

agreement for many resonance peaks, such as 12.4 eV and 19.3 eV in Fig. 12. The results indicate that the detection system is reliable.

5.2 Total cross sections of carbon

Given that the width of the proton beam pulse is 50 ns and the beam is in the double mode, it will cause superposition and broadening in the energy region above keV. The effect of the neutron energy spectrum measurement in double mode is approximately 1.8–8.8% in the energy range of 1–20 MeV. Therefore, the evaluated data cannot be directly compared to the experimental results. The carbon data evaluated in ENDF/B-VIII.0 were broadened using the Gaussian function as shown in Fig. 13. To achieve broadening, the energy total cross sections from ENDF/B-VIII.0 were initially converted into TOF total cross section with a flight path of $\sim$ 76 m and an energy range of 1–20 MeV. Each energy point was then broadened

using a standard normal distribution function with an FWHM of 52 ns and a pulse width of 50 ns. The resolution of the detector was 5.7 ns. The broadened data of the single bunch and the double bunch with an interval of 410 ns were then obtained. Finally, the broadened TOF total cross sections were converted into energy total cross section. From Fig. 13, a smaller cross section of resonance peaks can be seen in the broadened data, and it is caused by the FWHM of 50.3 ns, which is set in the calculation.

The presented results are compared with the broadened data in Fig. 14. In the energy range of 1–20 MeV, the measured neutron total cross sections with ^{235}U fission cells are in good agreement with that of the ^{238}U fission cells and the deviation is from 0.5 to 4.4%; it is generally less than 3%. The measured results with ^{235}U and ^{238}U cells are preliminary compared to the broadened data and the deviations are 0.5–9% and 0.4–9%, respectively. The experimental result is in good agreement with the evaluated data in ENDF/B-VIII.0 for the 2.077 MeV resonance peak.

5.3 Study on the separation of the measured spectra

Based on the unfolding procedure developed by the project team members, the separated neutron spectra were obtained. The unfolding procedure was developed based on the Bayesian principle. More detailed information on the procedure will be provided in an upcoming report that will be published by the project team members. Using the unfolding procedure, the neutron total cross section of the single bunch can be obtained, as shown in Fig. 15.

The neutron total cross section after unfolding is generally consistent with the broadened single-mode data. The results for the ^{238}U fission cells fluctuate greatly in the range of 1–1.5 MeV due to the insufficient fission count. In the energy region from 1 to 1.5 MeV, the count of a bin is from 39 counts to 987 counts and the average count is 255
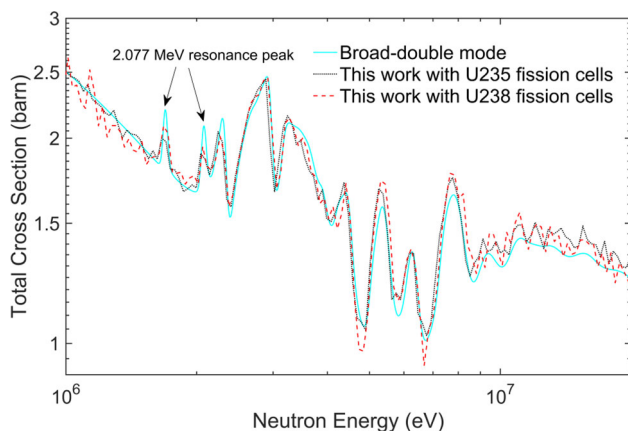

Fig. 14 The measured neutron total cross sections of natural carbon compared with the broadened data
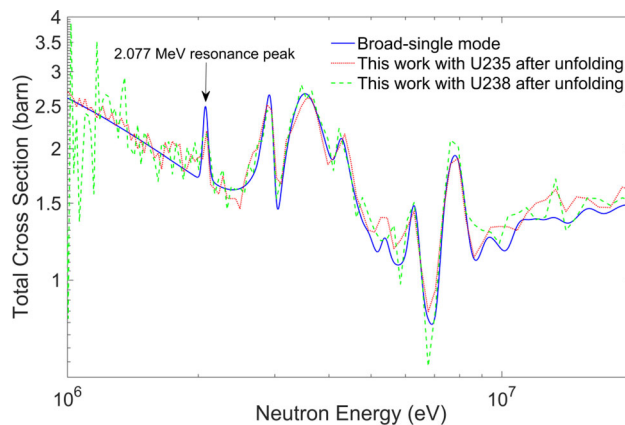

Fig. 15 The measured neutron total cross section (after unfolding) of natural carbon compared with the broadened data

counts/bin. Insufficient fission counts lead to a large error during unfolding. Given the time resolution of the fission chamber and the 50 ns proton bunch width, the 5 MeV and 5.37 MeV peaks are superimposed. Therefore, they are not easily identified in Fig. 15. There will be a dedicated short-bunch operation mode with a bunch length of 1.5 ns or 3.3 ns in rms in the future. For 1.5 ns, this corresponds to 0.1–0.6% in rms time resolution for the neutron energy from 10 keV to 100 MeV [10].

6 Conclusion

Based on the CSNS-WNS, NTOX has been established. The first measurement of the neutron total cross section of natural carbon in the energy region from 1 eV to 20 MeV was successfully performed using the neutron TOF method. A multilayer fast fission chamber with ^{235}U and ^{238}U was used as the neutron detector. The uncertainty due to counting statistics is generally approximately 3% for each bin in the energy range of 1–20 MeV. The measured total cross sections with ^{235}U fission cells are in good agreement with that with the ^{238}U fission cells. The deviation is generally less than 3%. The experimental results show that the detection system is reliable and feasible. By broadening the evaluated data in ENDF/B-VIII.0 using a Gaussian function, this work is preliminarily compared with the database in the energy range between 1 and 20 MeV and the deviation is generally 0.4–9%. The results show that NTOX can be used to measure the neutron total cross section of different samples at the CSNS-WNS in the future.

References

1. D.C. Larson, C.H. Johnson, J.A. Harvey et al., Measurement of the Neutron Total Cross Section of Fluorine from 5 eV to 20 MeV, Report No. ORNL-TM-5612 (1976)

2. Y. Danon, R.C. Block, M. Rapp et al., High-accuracy filtered neutron beam and high-energy transmission measurements at the Gaerttner Laboratory, in *Paper Presented at the 15th International Conference on Nuclear Data for Science and Technology* (Nice, France, 22–27 April 2007)

3. R.W. Finlay, W.P. Abfalterer, G. Fink et al., Neutron total cross sections at intermediate energies. Phys. Rev. C **47**, 237 (1993)

4. W.P. Abfalterer, R.W. Finlay, S.M. Grimes, Level widths and level densities of nuclei in the $32 \leq A \leq 60$ mass region inferred from fluctuation analysis of total neutron cross sections. Phys. Rev. C **62**, 064312 (2000). https://doi.org/10.1103/PhysRevC.62.064312

5. W.P. Abfalterer, F.B. Bateman, F.S. Dietrich et al., Measurement of neutron total cross sections up to 560 MeV. Phys. Rev. C **63**, 044608 (2001). https://doi.org/10.1103/PhysRevC.63.044608

6. M.J. Rapp, Y. Danon, F.J. Saglime et al., Beryllium and graphite neutron total cross-section measurements from 0.4 to 20 MeV. NSE **172**, 268–277 (2012). https://doi.org/10.13182/NSE11-55

7. S.X. Fang, Physics parameters and design study for the beijing spallation neutron source. J. Kor. Phys. Soc. **48**, 697 (2006)

8. J. Wei, H.S. Chen, Y.W. Chen et al., China spallation neutron source: design, R&D, and outlook. Nucl. Instrum. Method A **600**, 10 (2009). https://doi.org/10.1016/j.nima.2008.11.017

9. H. Chen, X.L. Wang, China's first pulsed neutron source. Nat. Mater. **15**, 689 (2016)

10. Q. An, H.Y. Bai, J. Bao et al., Back-n white neutron facility for nuclear data measurements at CSNS. JINST **12**, P07022 (2017). https://doi.org/10.1088/1748-0221/12/07/P07022

11. D.A. Brown, M.B. Chadwick, R. Capote et al., Nucl. Data Sheets **148**, 11 (2018). https://doi.org/10.1016/j.nds.2018.02.001

12. D.A. Brown, M.B. Chadwick, R. Capote et al., Nucl. Data Sheets **148**, 28 (2018). https://doi.org/10.1016/j.nds.2018.02.001

13. D.A. Brown, M.B. Chadwick, R. Capote et al., Nucl. Data Sheets **148**, 34 (2018). https://doi.org/10.1016/j.nds.2018.02.001

14. H.T. Jing, J.Y. Tang, H.Q. Tang et al., Studies of back-streaming white neutrons at CSNS. Nucl. Instrum. Method A **621**, 91–96 (2010). https://doi.org/10.1016/j.nima.2010.06.097

15. J. Ren, X.C. Ruan, H.Q. Tang et al., Simulation of the background of experimental end-stations and the collimator system of the CSNS back-streaming white neutron source. Nucl. Tech. **37**(10), 100521 (2014). https://doi.org/10.11889/j.0253-3219.2014.hjs.37.100521 **(in Chinese)**

16. J. Wen, Y. Wei, Z. Wen et al., A multi-layered fast ionization chamber prototype for fission cross section measurements. JINST **13**, P07020 (2018). https://doi.org/10.1088/1748-0221/13/07/P07020

17. Q. Wang, P. Cao, X. Qi et al., General-purpose readout electronics for white neutron source at China spallation neutron source. Rev. Sci. Instrum. **89**(1), 013511 (2018). https://doi.org/10.1063/1.5006346

18. Z.H. Wu (ed.), *Nuclear physics experiment method* (Atomic Energy Press, Beijing, 1997)

19. I. Antcheva, M. Ballintijn, B. Bellenot, et al., ROOT - A C++ framework for petabyte data storage, statistical analysis and visualization. Comput. Phys. Commun. **180**, 2499–2512 (2009)